

Irradiation study of liquid crystal variable retarder for Full-disk Magneto-Graph payload onboard ASO-S mission

Jun-Feng Hou(侯俊峰), Hai-Feng Wang(王海峰), Gang Wang(王刚), Yong-Quan Luo(骆永全), Hong-Wei Li(李宏伟), Zhen-Long Zhang(张振龙), Dong-Guang Wang(王东光), Yuan-Yong Deng(邓元勇)

Citation: Chin. Phys. B . 2020, 29(7): 074208 . **doi:** 10.1088/1674-1056/ab8c40
Journal homepage: http://cpb.iphy.ac.cn; http://iopscience.iop.org/cpb

What follows is a list of articles you may be interested in

Gastroscopy-conjugated photoacoustic and ultrasonic dual-mode imaging for detection of submucosal gastric cancer: *in vitro* study

Huaqin Wu(吴华钦), Haiyang Song(宋海洋), Yudian Huang(黄玉钿), Zhifang Li(李志芳), Shulian Wu(吴淑莲), Xiaoman Zhang(章小曼), Hui Li(李晖)

Chin. Phys. B . 2020, 29(6): 064205 . **doi:** 10.1088/1674-1056/ab84d4

Internal and near-surface fields for a chiral sphere under arbitrary laser beam illumination

Bi-Da Su(苏必达), Ming-Jun Wang(王明军), Yue Peng(彭月), Su-Hui Yang(杨苏辉), Hua-Yong Zhang(张华永)

Chin. Phys. B . 2019, 28(6): 064210 . **doi:** 10.1088/1674-1056/28/6/064210

Laser-induced damage threshold in HfO_2/SiO_2 multilayer films irradiated by β-ray

Mei-Hua Fang(方美华), Peng-Yu Tian(田鹏宇), Mao-Dong Zhu(朱茂东), Hong-Ji Qi(齐红基), Tao Fei(费涛), Jin-Peng Lv(吕金鹏), Hui-Ping Liu(刘会平)

Chin. Phys. B . 2019, 28(2): 024215 . **doi:** 10.1088/1674-1056/28/2/024215

Spectroscopic and radiation-resistant properties of Er, Pr: GYSGG laser crystal operated at 2.79μm

Xu-Yao Zhao(赵绪尧), Dun-Lu Sun(孙敦陆), Jian-Qiao Luo(罗建乔), Hui-Li Zhang(张会丽), Zhong-Qing Fang(方忠庆), Cong Quan(权聪), Xiu-Li Li(李秀丽), Mao-Jie Cheng(程毛杰), Qing-Li Zhang(张庆礼), Shao-Tang Yin(殷绍唐)

Chin. Phys. B . 2017, 26(7): 074217 . **doi:** 10.1088/1674-1056/26/7/074217

Irradiation effect on strain sensitivity coefficient of strain sensing fiber Bragg gratings

Jin Jing, Lin Song, Song Ning-Fang

Chin. Phys. B . 2014, 23(1): 014206 . **doi:** 10.1088/1674-1056/23/1/014206

Irradiation study of liquid crystal variable retarder for Full-disk Magneto-Graph payload onboard ASO-S mission*

Jun-Feng Hou(侯俊峰)[1,4,†], Hai-Feng Wang(王海峰)[2], Gang Wang(王刚)[1,4], Yong-Quan Luo(骆永全)[2], Hong-Wei Li(李宏伟)[3], Zhen-Long Zhang(张振龙)[3], Dong-Guang Wang(王东光)[1], and Yuan-Yong Deng(邓元勇)[1,4]

[1] *Key Laboratory of Solar Activity, National Astronomical Observatories, Chinese Academy of Sciences, Beijing* 100101, *China*
[2] *Institute of Fluid Physics, China Academy of Engineering Physics, Mianyang* 621900, *China*
[3] *National Space Science Center, Chinese Academy of Sciences, Beijing* 100190, *China*
[4] *School of Astronomy and Space Science, University of Chinese Academy of Sciences, Beijing* 101408, *China*

(Received 9 March 2020; revised manuscript received 17 April 2020; accepted manuscript online 23 April 2020)

The Advanced Space-based Solar Observatory (ASO-S) is a mission proposed by the Chinese Solar Physics Community. As one of the three payloads of ASO-S, the Full-disc Magneto-Graph (FMG) will measure the photospheric magnetic fields of the entire solar disk with high spatial and temporal resolution, and high magnetic sensitivity, where liquid crystal variable retarder (LCVR) is the key to whether FMG can achieve its scientific goal. So far, there is no space flight experience for LCVR. Therefore, irradiation study for LCVRs becomes more important and urgent in order to make sure their safety and reliability in space application. In this paper, γ irradiation, proton irradiation, and ultra-violet (UV) irradiation are tested for LCVRs respectively. The optical and chemical properties during irradiation tests are measured and analyzed. For optical properties, there is no significant change in those parameters FMG payload concerned except the retardation. Although there is no drastic degradation in the retardation *versus* voltage during irradiations, the amount of retardation variation is much higher than the instrument requirements. Thus, an in-flight retardation *versus* voltage should be added in FMG payload, reducing or even avoiding the impact of retardation change. For chemical properties, the clearing point and birefringence of the LC materials almost have no change; the ion density dose not change below 60 krad[Si], but begin to increase dramatically above 60 krad[Si].

Keywords: solar telescope, liquid crystal variable retarder (LCVR), irradiation

PACS: 42.88.+h, 42.70.Df, 95.55.Ev, 95.55.Fw **DOI:** 10.1088/1674-1056/ab8c40

1. Introduction

The Advanced Space-based Solar Observatory (ASO-S)[1] is a mission proposed for the 25th solar maximum by the Chinese Solar Physics Community. This mission is supported by the Chinese Academy of Sciences (CAS) Strategic Pioneer Program on Space Science and is scheduled to be launched at the end of 2021 or early 2022.

Being the first approved Chinese Solar Satellite, ASO-S will focus on observing solar magnetic fields, solar flares, and coronal mass ejections (CMEs) simultaneously, in order to study the relationships between the solar magnetic field, solar flares, and CMEs, which are the key scientific questions in modern solar physics.[2–5] Where the magnetic field is the preferred physical parameter measured by ASO-S. As one of three payloads, the Full-disc Magneto-Graph (FMG) will measure the photospheric magnetic fields of the entire solar disk with high spatial and temporal resolution, and high magnetic sensitivity.[2]

Solar magnetic field, especially in photosphere, is measured by polarimetry based on Zeeman effect and polarized radiation transfer theory of solar atmosphere.[6,7] Thus, solar magnetic field measurement is actually a polarization measurement for solar telescopes, and polarimetry is the key to magnetic field measurement by solar telescopes,[8–13] no exception for FMG.

FMG is a full-disk vector magnetic fields telescope with an aperture 140 mm and working spectra line Fe I 532.4 nm. Both liquid crystal variable retarders (LCVRs) are utilized in Stokes polarimeter of FMG to improve polarization sensitivity. LCVR is envisaged as a promising novel technique for polarization measurement in space applications due to the inherent advantage of eliminating the need for conventional rotating polarizing optics and increasing the measuring speed.[14,15] However, any onboard element used for aerospace applications must be space qualified; *i.e.*, it must be able to survive the hazards of operation in space due to harsh space radiation environmental conditions, and it must be low risk. So far, there is no space flight experience for LCVRs, therefore irradiation tests for LCVRs become more important than traditional mechanic mode.

A few irradiation tests have been done in the past to verify the spatial adaptability of LCVRs.[16–23] Heredero, Patarroyo,

*Project supported by the Strategic Pioneer Program on Space Science, Chinese Academy of Sciences (Grant Nos. XDA15010800 and XDA15320102) and the National Natural Science Foundation of China (Grant Nos. 11427901, 11773040, 11403047, and 11427803).

†Corresponding author. E-mail: jfhou@bao.ac.cn

© 2020 Chinese Physical Society and IOP Publishing Ltd

Belenguer *et al.*[16] have done the γ and UV irradiations tests of LCVRs in 2007 for the Imaging Magnetograph eXperiment (IMaX), which is one of the three instruments of the payload of the SUNRISE balloon project within the NASA Long Duration Balloon program. Herrero, Patarroyo and Parejo *et al.* reported γ, proton, and UV irradiations tests of LCVRs in 2011 for Solar Orbiter space mission.[17] However, no driving voltage had been applied to LCVRs in these irradiation tests. But for an elctro-optic modulation device, the irradiation characteristic of LCVRs with and without derived voltages during irradiations is also a key point needed to research.

In this paper, the radiation effects of LCVRs used in FMG payload are systematically studied. The main purpose of this study is to test and analyze whether the performance changes of LCVRs under various irradiations can meet the scientific requirements of FMG, and to give the corresponding strategies. The results are also expected to be helpful to developing some other relevant LCVRs-based aerospace instruments.

2. Radiation dose analysis of LCVR in FMG

2.1. Construction of LCVR[16]

An LCVR consists of a nematic liquid-crystal (LC) material layer sandwiched between two fused-silica substrates (illustrated in Fig. 1). The outer surfaces of both substrates are coated with an antireflective film to reduce reflection. The inner surfaces of both substrates are coated with a transparent indium tin oxide (ITO) electrode and a polyimide layer in turn. Some spacers are used to control the thickness of the liquid crystal accurately. The polyimide layer forces an initial orientation of the LC molecules in *a* direction parallel to that of the silica plates, which define the optics axis of LCVR. The application of a voltage through the ITO films generates a homogeneous electric field inside the cavity that forces the LC molecules to tilt to a given angle with respect to the substrate surface. Thus the birefringence index is changed, and the retardations of LCVR will vary with the voltages (as shown in Fig. 2). In other words, LCVR is an electro-optic modulator, and it can modulate the linear polarization to circular or *vice versa* by changing the voltage.

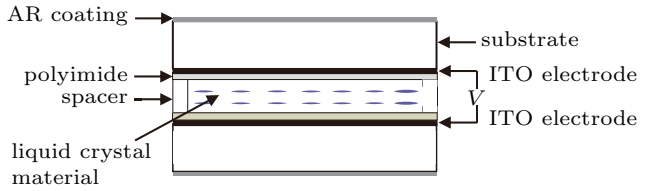


Fig. 1. The construction of LCVR.

Table 1 lists the materials, refractive index, and thicknesses of the LCVR we have used in FMG, which is manufactured by Institute of Fluid Physics, China Academy of Engineering Physics. The liquid crystal molecule is a kind of mixture materials 5CB(PP5CN), taking 5CB as the main. Its molecular structure is shown in Fig. 3.

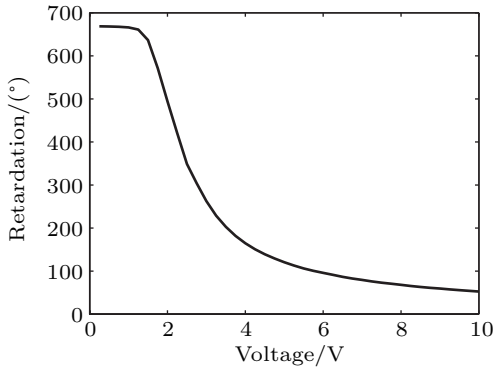


Fig. 2. The relations of retardation of LCVR with voltages.

Table 1. Materials, refractive index, and thickness of LCVR in FMG.

Material	Refractive index	Thickness
Fused silicon	$n_o = 1.46$	5 mm
ITO	$n_o = 2.0$	50 nm
Polyimide	$n_o = 1.5$	300 nm
Liquid crystal	$n_o = 1.5$, $n_e = 1.76$	5 μm

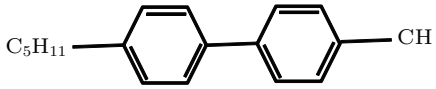


Fig. 3. Molecular structure of liquid crystal used in FMG.

2.2. Radiation dose analysis of LCVR in FMG

ASO-S will be launched to a Sun-synchronous orbit (SSO) at an attitude of 720 km. The harsh space environments on the orbit are the radiation belts protons, the radiation belts electrons, solar protons, UV radiation, atomic oxygen, and space debris. It is difficult for atomic oxygen and space debris to get inside of optic box of FMG, so what we need to consider is the influence of the radiation belts protons, the radiation belts electrons, solar protons and UV radiation on LCVRs. According to the structure characteristics and operating principle of LCVR and analysis of environmental effects of space radiation, the possible impacts and dose are as follows.

2.2.1. Total ionization dose effect

Energy will be deposited when high-energy protons and electrons pass through LCVR, which will lead to the ionization of nearby atoms and produce electrons and ions. The energy is total ionization dose. The poor conductivity of LCVR makes the electrons and ions difficult to rapidly compound, and then a new electric dipole moment is formed within LCVR. The new electric dipole moment may affect the effective voltage added to LCVR, thus changing the relations of phase retardation with derived voltages. The total ionization dose incidence in LCVR is about 9.6 krad[Si] and 20.7 krad[Si] at 5-year and 11-year

respectively, where 5-year is the ASO-S design lifetime and 11-year is a solar cycle we hope ASO-S can work.

2.2.2. Displacement damage effect

The collision between high-energy protons and molecules of liquid crystal materials may lead to the displacement of atoms, changing the properties of LCVR. The energy doposied by the collision is the displacement damage dose. The dose of displacement damage of LCVR is 2.4×10^8 MeV/g and 5.3×10^8 MeV/g at 5-year and 11-year, respectively.

2.2.3. Charging effect

High-energy electrons are deposited in the liquid crystal material or on the substrate of LCVR, which will lead to the continuous accumulation of electrons and form the charging effect. The charging will counteract or enhance the applied voltage when the LCVR works, hence changing the polarization characteristics of LCVR. The equilibrium potential of charging is about 1.8×10^{-6} V after calculation, which is far less than the required voltage accuracy 0.001 V of LCVR. The possible reason is that our satellite orbit is relatively low and the flux of high-energy electrons on the LCVR is so small that the charging effect is week. But the effect has to be focused on high orbit as geosynchronous orbit.

2.2.4. UV irradiation

Because FMG is a solar telescope, UV radiation must be taken into account. Moreover, LC material is also sensitive to UV spectra. The ultraviolet irradiation may change the chemical properties of LCVR, leading to performance degradation. In order to reduce the influence of UV radiation and stray light on FMG, a front widow with a pass band 532.4 nm$\pm$5 nm is designed and used to prevent the light from other wavelengths entering the optical system. The transmittance of front window is given Fig. 4. There is a peak near 370 nm and 200 nm respectively, where the peak near 370 nm is a real sub-maximum from coatings of the front widow, but another one near 200 nm is from measurement error and can be ignored. Finally, the UV radiation dose of LCVR is about 2.5×10^{-4} ESH at [200 nm 360 nm] and 13.3 ESH at [360 nm 400 nm] over 11-year.

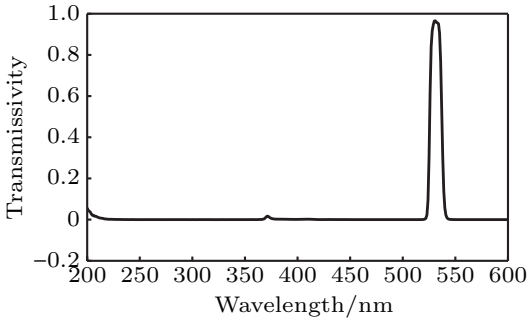


Fig. 4. Transmissivity of the front widow in FMG.

Table 2 lists the main radiation effects and dose we need to test in LCVR of FMG according to the above analysis. Three kinds of radiation resources, γ radiation resource and high-energy proton and UV lamps, were used to done the test for total ionization dose effect, displacement damage effect, and UV irradiation respectively.

Table 2. The main radiation effects and dose of LCVR in FMG.

Radiation effects	Dose
Total ionization dose	20.7 krad[Si]
Displacement damage	5.3×10^8 MeV/g or 21.2×10^{10} p/cm^2
UV radiation	2.5×10^{-4} ESH @[200 nm 360 nm]
	13.3 ESH @[360 nm 400 nm]

3. Irradiation test procedures

3.1. Samples and experimental setup

A total of twelve identical LCVRs were used for irradiation testing: four LCVRs for γ irradiation (LCVR#1–LCVR#4), three for proton irradiation (LCVR#5–LCVR#7), and four for UV irradiation (LCVR#8–LCVR#11). The remaining one sample (LCVR#12) was designated as controls and was not exposed to any irradiation but was shipped between locations together with the irradiation samples to make their history as similar as possible. Besides, seven identical liquid crystal (LC) materials were exposed to γ irradiation to test the material's chemical properties.

To verify the fulfilment of LCVRs requirements for FMG the following seven key parameters were measured in irradiation experiments:

(i) Retardation *versus* voltage;
(ii) Response time;
(iii) Transmission;
(iv) Transmitted wavefront error;
(v) Clearing point;
(vi) Birefringence;
(vii) Ion concentration.

The first four parameters represent the optical properties of LCVRs and the last three represent the chemical properties of LC material we used.

All the parameters were not measured *in situ*. In each irradiation, parameters (i)–(iii) had to be measured during all the intermediate doses, the time-lapse from the start of the optical parameters measurements to the start of the next irradiation exposure (another intermediate doses) is limited to one hour. By contrast, parameter (iv) was measured only before and after each irradiation test and parameters (iv)–(vii) measured only after γ irradiation test.

The experimental setups employed to measure all the optical parameters included an automatic retardation-voltage measurement system that can measure retardation–voltage curves and response time, a transmission measuring system with fiber-spectrometer and a Zygo interferometer. Response time was required to measure at 35 ℃ where LCVRs work in FMG. The other parameters were measured in room temperature.

The LCs samples after γ irradiation were measured by Xi'an Modern Chemistry Research Institute to test the chemical change of LCVRs, including clearing point and birefringence and ion concentration.

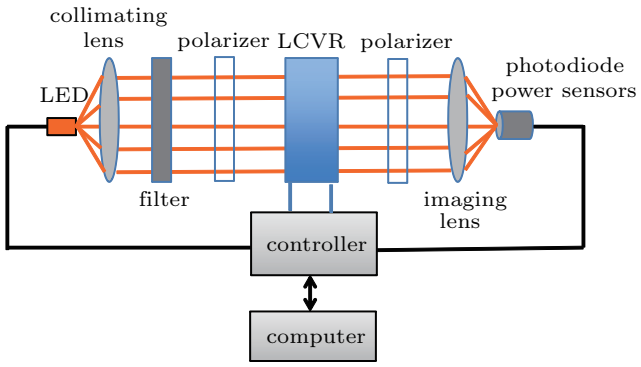


Fig. 5. An automatic retardation–voltage measurement system.

It is noted that, a simple, fast but robust method was applied to measure retardation–voltage curves in the automatic retardation–voltage measurement system as shown in Fig. 5. The transmission directions of both polarizers are parallel, and the optic axis of LCVR is set at 45° relative to the polarizer. The retardation, corresponding to each driving voltage, is related to the detection intensity as $I_V = I_o\cos^2(\delta/2)$. Thus, retardation–voltage curves will be easy to calculate. In addition, we have carried out a lot of stability tests and comparison with the Soleil compensation method in the laboratory, and made sure the measurement accuracy within ±1°, meeting the requirements of this irradiation tests.

3.2. γ irradiation

The γ irradiation was tested in Peking University (Fig. 6(a)). A ^{60}Co source was used at atmospheric pressure and room temperature. The samples under irradiation included 2 LCVRs with derived voltage during irradiation, 2 LCVRs without derived voltage, and 6 homologous LC materials. Besides, another LC material was used as a reference without irradiation. The samples were undergone to 6 intermediate doses in order to assess the tolerance of the LCVRs to ionizing radiation. Table 3 lists the intermediate doses and dose rates for all the samples received, where "Y" indicates the sample underwent the corresponding intermediate dose point, but "N" not.

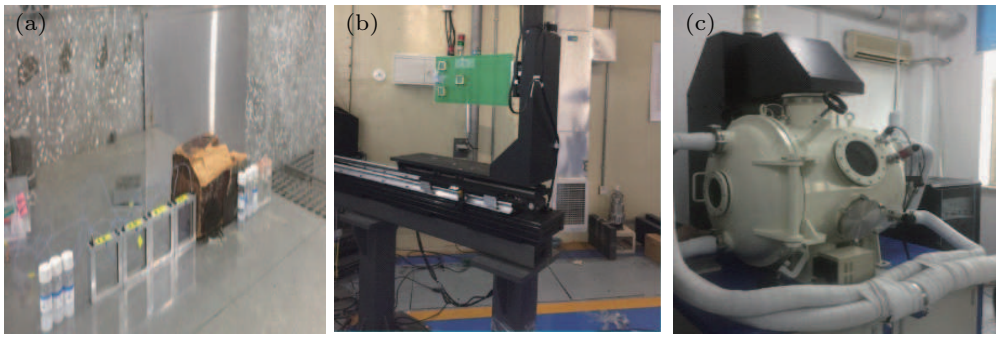


Fig. 6. Radiation test pictures: (a) γ irradiation; (b) proton irradiation; (c) UV irradiation.

Table 3. The intermediate doses and dose rates for all the samples received in γ irradiation.

Dose/krad	Dose rate/(krad/h)	Samples									
		LCVR#1 without voltage	LCVR#2 without voltage	LCVR#3 with voltage	LCVR#4 with voltage	LC#2	LC#3	LC#4	LC#5	LC#6	LC#7
4	5	Y	Y	Y	Y	Y	Y	Y	Y	Y	Y
10	5	Y	Y	Y	Y	N	Y	Y	Y	Y	Y
20	5	Y	Y	Y	Y	N	N	Y	Y	Y	Y
60	36	Y	Y	Y	Y	N	N	N	Y	Y	Y
130	5	Y	Y	Y	Y	N	N	N	N	Y	Y
500	180	Y	N	Y	N	N	N	N	N	N	Y

3.3. Proton irradiation

The proton irradiation was tested at 100-MeV compact cyclotron (CYCIAE-100) in China Institute of Atomic Energy (Fig. 6(b)). The samples under irradiation include two LCVRs without derived voltage and one with derived voltage. Table 4 lists the intermediate doses and dose rates for all the samples received as Table 3.

Table 4. The intermediate doses and dose rates for all the samples received in proton irradiation.

Dose /(10^{10} p/cm^2)	Dose rate /(10^7 p/cm$^2\cdot$s)	Samples		
		LCVR#5 without voltage	LCVR#6 without voltage	LCVR#7 with voltage
5	2	Y	Y	Y
10	2	Y	Y	Y
20	2	Y	Y	Y
50	20	Y	Y	Y
100	20	Y	N	Y

3.4. UV irradiation

The UV irradiation was tested in Harbin Industrial University (as shown in Fig. 6(c)). The three LCVRs are irradiated at a vacuum ultraviolet irradiation setup in the spectral range of [200 400] nm. However, it is known from Table 2 that the UV radiation of FMG may mainly come from the spectra range of [360 400] nm. Therefore, another LCVR is irradiated by a narrowband UV light with center wavelengths at 365 nm to verify its characteristics.

Table 5. The intermediate doses and dose rates for all the samples received in the vacuum ultra-violet irradiation setup at the spectral range of [200 400] nm.

Dose/ESH	Dose rate/(ESH/h)	Samples		
		LCVR#8 without voltage	LCVR#9 without voltage	LCVR#10 without voltage
0.25	3	Y	Y	Y
0.50	3	Y	Y	Y
0.75	3	Y	Y	Y
1.00	3	Y	Y	Y
2.00	3	Y	Y	Y
5.00	3	Y	Y	Y

Table 6. The intermediate doses and dose rates of sample received in narrow band UV light with centre wavelengths at 365 nm.

Dose/ESH	Dose rate/(ESH/h)	Sample
		LCVR#11 without voltage
2.8	8.5	Y
5.6	8.5	Y
8.5	8.5	Y
11.3	8.5	Y
14.1	8.5	Y
16.9	8.5	Y

Tables 5 and 6 list the intermediate doses and dose rates for all the samples received in both UV irradiation tests.

4. Results and discussions

4.1. Retardation *versus* voltage

Figure 7 gives the optical retardation variation, relative to those before tests, *versus* applied voltage measured for all the 11 LCVR samples irradiated. No significant changes were found after irradiations except for proton irradiation.

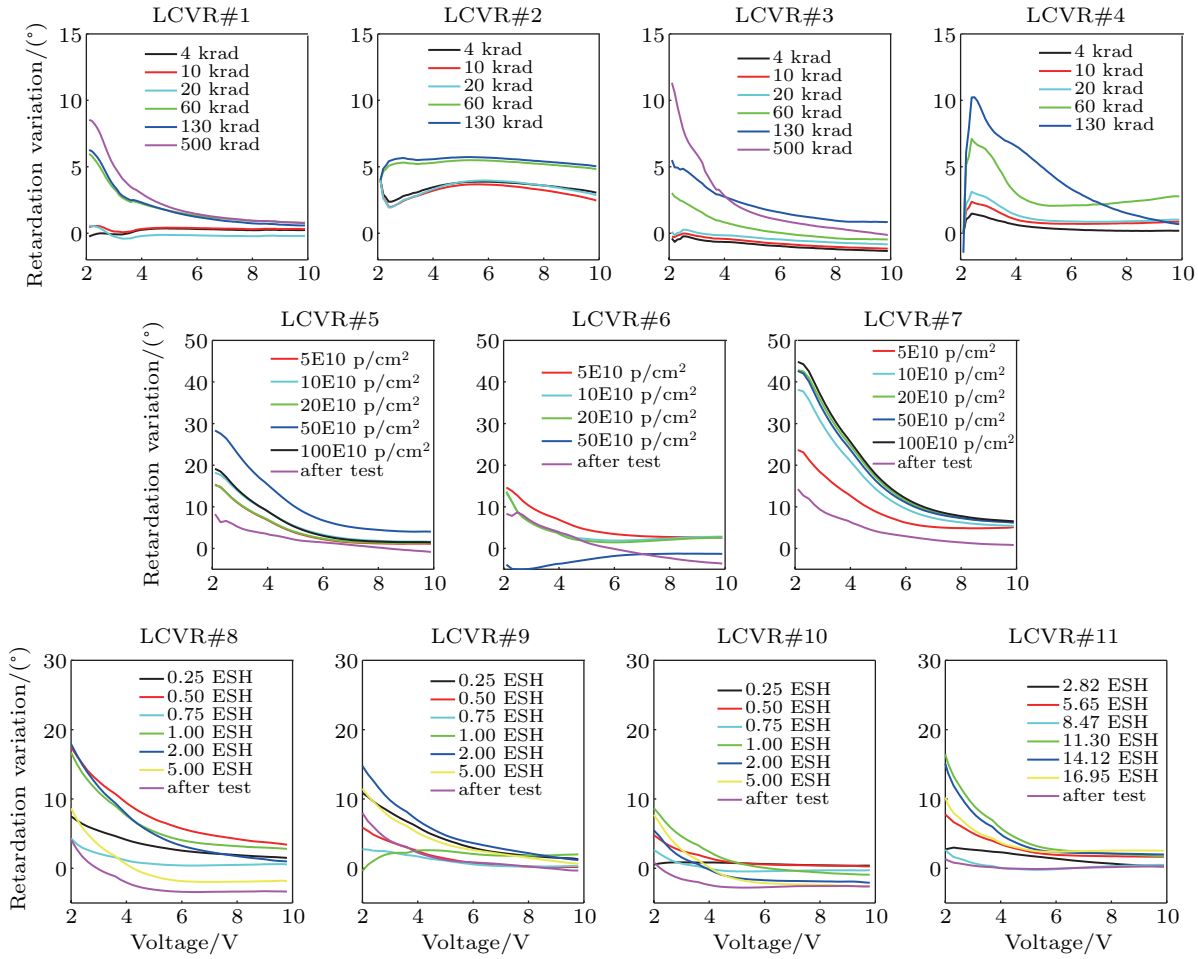


Fig. 7. Retardation variation curves *versus* applied voltage for all the 11 samples irradiated. In the figure, the abbreviation of number 5E10 means 5×10^{10}.

In order to analyze these changes in detail we got the retardation variation curves with irradiation dose for every sample by only extracting one voltage point from each sample. The voltage value chosen corresponds to the retardation about 360°, which is the most sensitive position to irradiation over the retardation range of 90°–360° and can completely represent the trend of the whole retardation–voltage curve we need. The results are shown in Fig. 8, where the first column indicates the retardation

variation and the second column indicates the corresponding variation rates. It should be noted that the logarithmic coordinate (x axis) is selected in the first three rows for the sake of clear display.

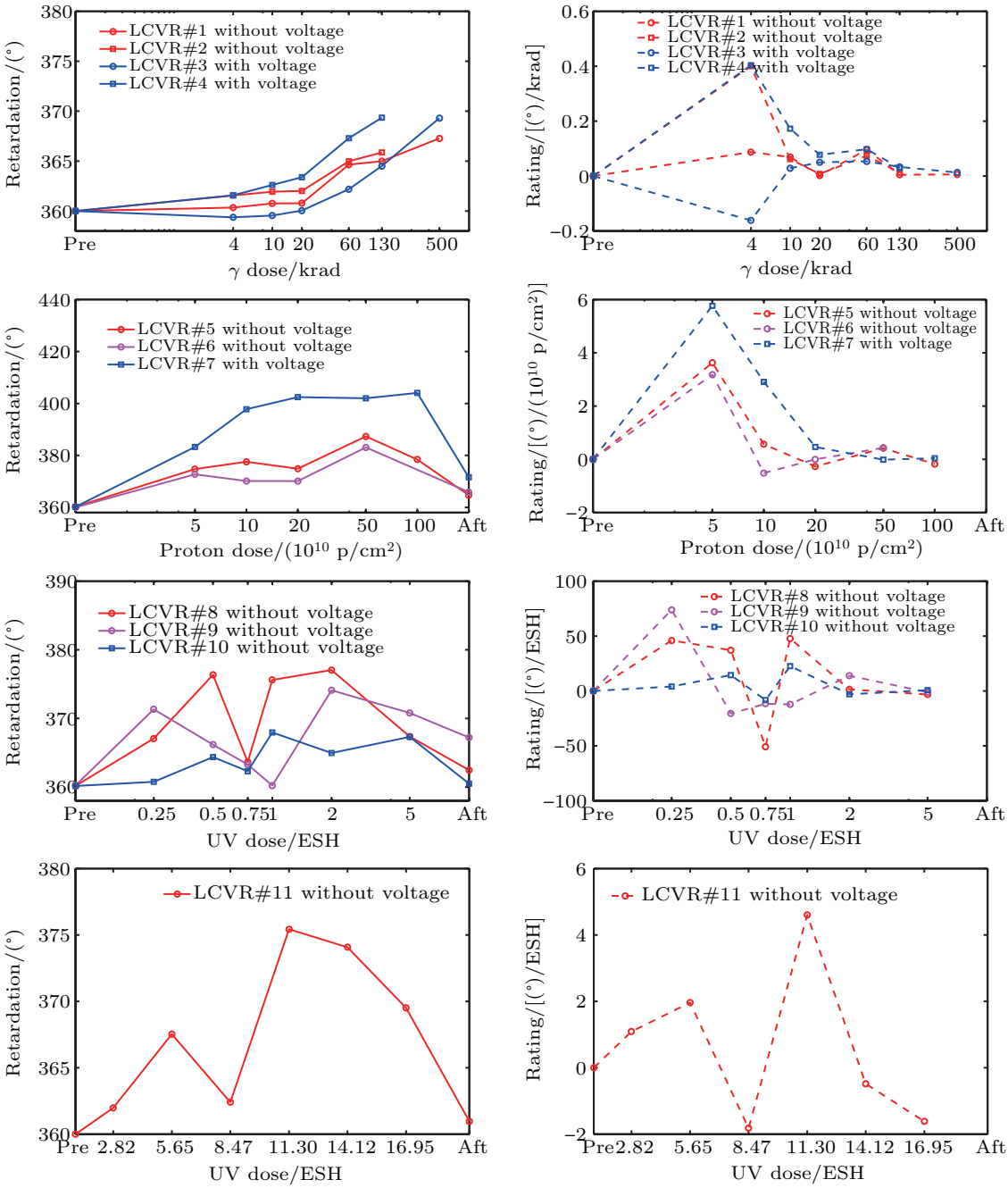


Fig. 8. Retardation variation with irradiated dose. In the figures, "Pre" means before the irradiation test and "Aft" means after the irradiation test.

4.1.1. γ irradiation

The first row in Fig. 8 shows the retardation and variation rates measured after the LCVRs have been irradiated by γ with 4, 10, 20, 60, 130, and 500 krad. It can be observed that: i) The retardation changes about 1% after 20 krad and 2.7% after 500 krad, the variation is very small; ii) The larger the dose, the slower the rate of change; iii) The measurement results are not significantly different regardless of whether samples are derived by voltage during irradiation.

4.1.2. Proton irradiation

The second row shows the retardation and variation rates measured after the LCVRs have been irradiated by proton with 5×10^{10}, 10×10^{10}, 20×10^{10}, 50×10^{10}, and 100×10^{10} p/cm^2. It can be found that: i) All the samples have the same trend with proton dose no mater with voltage or not during irradiation; ii) The larger the dose, the slower the rate of change; iii) The retardation of the sample with voltage during irradiation changes about 11.1%, almost twice as large as those of samples without voltage; iv) The retardation changes

rapidly before 10×10^{10} p/cm^2, then it reaches saturation but can return to original value after completing proton irradiation (measured again three days after the end of the irradiation).

4.1.3. UV irradiation

The last two rows show the retardation and variation rates measured after the LCVRs have been irradiated by UV light in the spectra ranges of [200 400] nm and [360 400] nm respectively. The main results are the following ones: A strange phenomenon is found that the retardation goes through two cycles of increase and decrease. The largest change is about 4.2%. The retardation measured 12 hours after the end of the UV irradiation has a tendency trying to return to its original state.

4.2. Response time

The response time is defined as the time needed for the LCVR to reach a second polarization state defined by voltage applied to the LCVR V_1 from the first polarization state defined by voltage V_2.

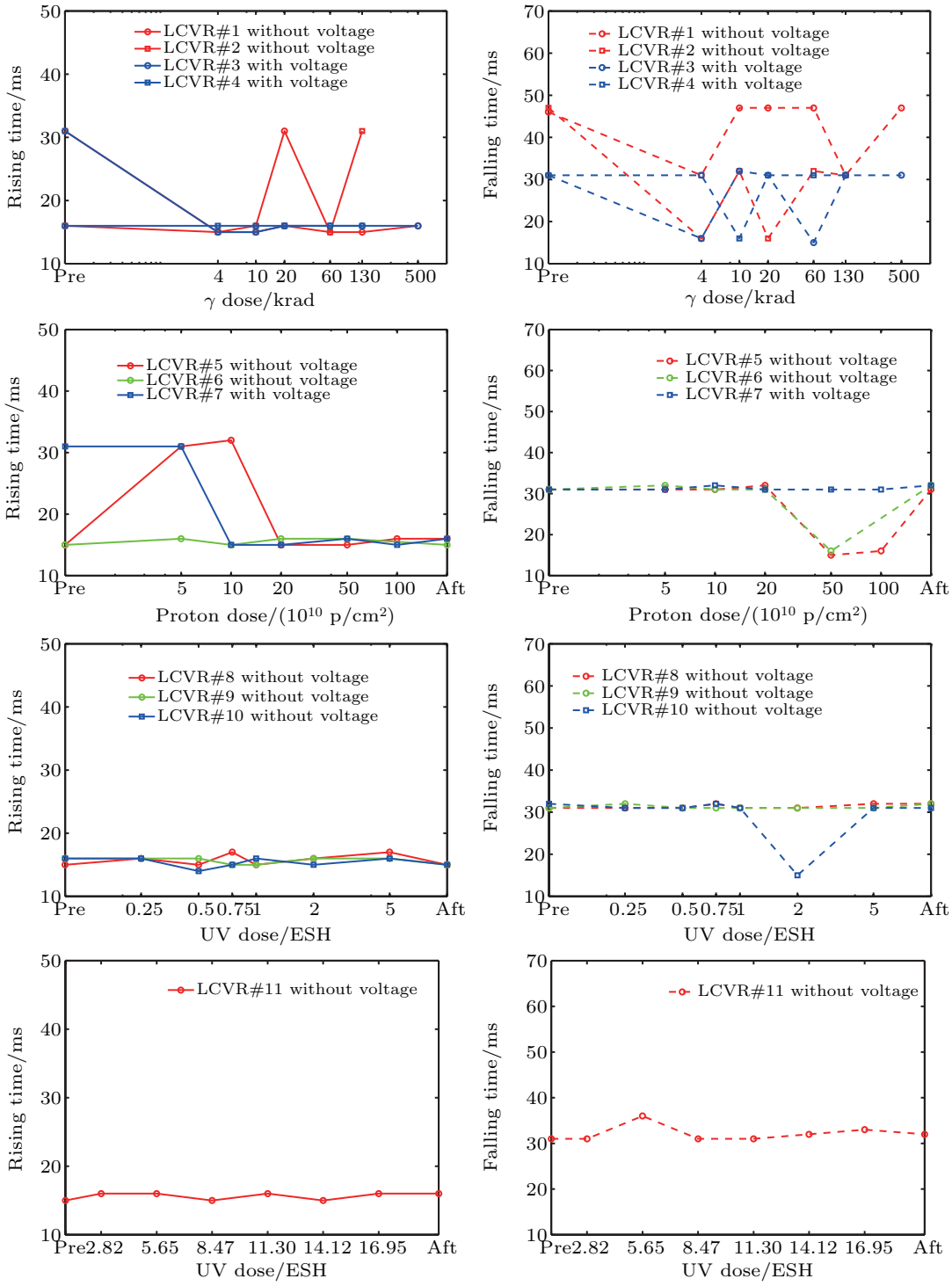


Fig. 9. Response time *versus* irradiated dose.

In irradiation testing, the exposure time is 1 ms; V_1 and V_2 are set in 2 V and 5 V respectively, which corresponds to the retardation about 360° and 90°. The measured results are shown in Fig. 9.

It is observed that: the rising time from V_1 to V_2 (<32 ms) is significantly less than the falling time from V_2 to V_1 (<50 ms). There are three typical response times found in the measurements, 16 ms, 32 ms, and 47 ms. They are almost multiple relationships, which are very interesting phenomena that deserve further study. However, there was no obvious change in response time before and after the irradiation test. The response time is less than 50 ms, meeting the scientific requirements of FMG payload.

4.3. Transmittance

Figure 10 represents the transmittance of each sample *versus* irradiated dose. The reason why the transmission oscillates with wavelength mainly comes from the mismatch of the refractive index of the TIO film and polyimide in LCVR. There is no obvious degradation during irradiation tests.

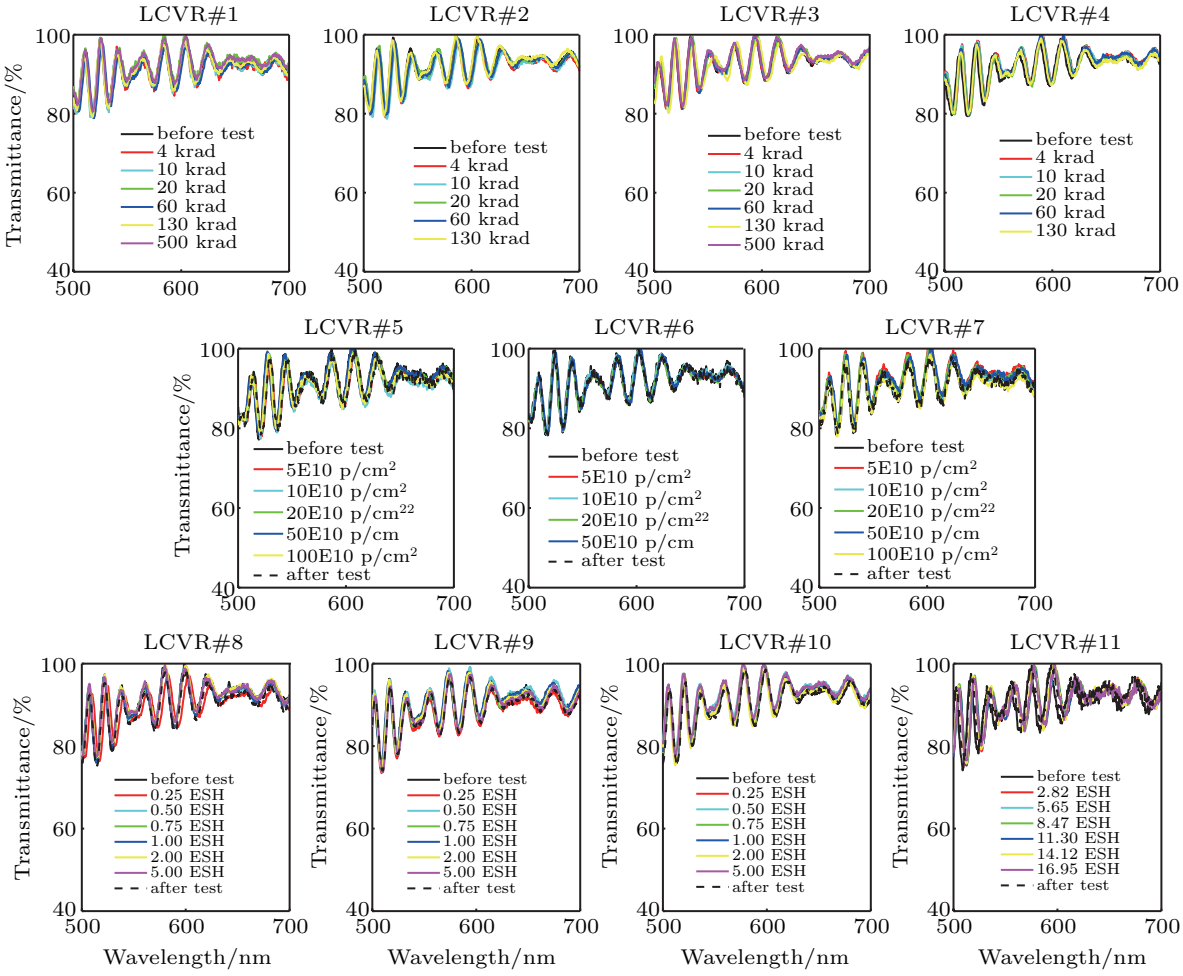


Fig. 10. Transmittance *versus* irradiated dose.

4.4. Wavefront error

The main results for wavefront error of all the samples can be seen in Table 7. There is no regular change, and the largest variation before and after irradiation tests is 0.089λ for PV and 0.013λ for RMS.

4.5. Chemical properties

Tables 8 and 9 display the results of chemical properties measured by Xi'an Modern Chemistry Research Institute, including clearing point, birefringence, and ion density. The clearing point is defined as a temperature at which the liquid crystal material is transparent during the process of changing from liquid crystal state to isotropic liquids state, representing the chemical performance; the birefringence index Δn represents the polarization properties; and the ion density represents the possible variation of voltage added to LCVR. The main results from Tables 8 and 9 are the following ones by comparing with reference sample LC#1: i) There is no obvious change for clearing point and birefringence index Δn before and after γ irradiation; ii) The ION almost has no significant variation below 60 krad, but begin to increase dramatically above 60 krad.

Table 7. The wavefront error of all the samples before and after irradiation tests.

Samples	Before		After		Variation	
	PV(λ)	RMS(λ)	PV(λ)	RMS(λ)	PV(λ)	RMS(λ)
LCVR#1	0.220	0.020	0.114	0.016	−0.106	−0.004
LCVR#2	0.120	0.015	0.128	0.023	0.008	0.008
LCVR#3	0.258	0.033	0.169	0.021	−0.089	−0.012
LCVR#4	0.119	0.020	0.080	0.014	−0.039	−0.006
LCVR#5	0.177	0.033	0.150	0.025	−0.027	−0.008
LCVR#6	0.135	0.040	0.172	0.027	0.037	−0.013
LCVR#7	0.252	0.050	0.227	0.054	−0.025	0.004
LCVR#8	0.096	0.013	0.086	0.015	−0.010	0.002
LCVR#9	0.110	0.017	0.093	0.011	−0.017	−0.006
LCVR#10	0.149	0.029	0.151	0.033	0.002	0.004
LCVR#11	0.206	0.034	0.184	0.022	−0.022	−0.012

Table 8. The clearing point and birefringence Δn of LCs after γ irradiation.

Samples	Dose/krad	Clearing point (start/peak)/°C	Δn @25°C, 589 nm
LC#1-ref	0	82.90/83.62	0.2451
LC#2	4	81.89/84.37	0.2451
LC#3	10	82.81/83.69	0.2454
LC#4	20	82.59/83.46	0.2453
LC#5	60	82.67/83.52	0.2453
LC#6	130	82.58/83.62	0.2452
LC#7	500	82.37/83.52	0.2452

Table 9. The ion density of LCs measured after γ irradiation.

Samples	Dose/krad	ION
LC#1-ref	0	27.66
LC#2	4	27.18
LC#3	10	28.02
LC#4	20	28.52
LC#5	60	27.15
LC#6	130	31.29
LC#7	500	37.57

4.6. Discussion

For optical properties of LCVR, error requirements for LCVR are listed in Table 10 in order to meet the scientific goals of FMG payload. It is easy to find out that the main error comes from retardation change. Although there was no drastic change in the retardation *versus* voltage during three irradiation processes, the amount of retardation change was still much higher than the instrument requirements. It has to be taken into account that an in-flight retardation *versus* voltage calibration method should be added in FMG payload, reducing or even avoiding the impact of retardation change.

Table 10. Error requirements for LCVR in FMG payload.

Parameter	Requirement
Retardation change	$\leq 0.6\%$
Response time	≤ 50 ms
Wavefront error variation	$\leq 0.025\lambda$ (RMS)
Transmission change	$\leq 10\%$

For chemical properties of LCVR, the measured results in Tables 8 and 9 show that we do not need to care about LC's chemical changes below 60-krad γ-irradiation doses.

5. Conclusion and perspectives

In this paper, space radiation effects and the equivalent dose of LCVR in FMG were analyzed and calculated firstly; based on that, γ irradiation, proton irradiation, and UV irradiation were tested for LCVRs respectively. The optical and chemical properties during irradiation tests were measured and analyzed. Some results are given below.

(I) For optical properties, there is no significant change in those parameters for FMG payload concerned except the retardation.

(II) For retardation, the amount of retardation change is still much higher than the instrument requirements though there is no drastic change in the retardation *versus* voltage during three irradiation processes.

(III) For chemical properties, the clearing point and birefringence of the LC materials almost have no change; the ion density does not change below 60 krad[Si], but begins to increase dramatically above 60 krad[Si].

Besides, some more interesting phenomena are also found:

I) The retardation changes in proton irradiation are obviously larger than those in γ and UV irradiations; the retardation of the samples with voltage during proton irradiation changes about 11.1%, almost twice as large as those of samples without voltage.

II) The retardation measured after the end of the proton and UV irradiations has a tendency trying to return to its original state. The most possible reason is that the irradiations mainly alter the effective electric field inside LCVR. After the irradiation is finished, the retardation gradually reverts to the initial value with the attenuation of the additional electric field.

III) There are three typical response times found in the measurements, 16 ms, 32 ms, and 47 ms. They are almost multiple relationships, which are very interesting phenomena that deserve further study.

References

[1] Gan W Q, Zhu Ch, Deng Y Y, *et al*. 2019 *RAA* **19** 156
[2] Deng Y Y, Zhang H Y, Yang J F, *et al*. 2019 *RAA* **19** 157
[3] Li H, Chen B, Feng L, *et al*. 2019 *RAA* **19** 158
[4] Chen B, Li H, Song K F, *et al*. 2019 *RAA* **19** 159
[5] Zhang Z, Chen D Y, Wu J, *et al*. 2019 *RAA* **19** 160
[6] Hale G E 1908 *ApJ* **28** 315
[7] Unno W 1956 *PASJ* **8** 108
[8] Keil S, Rimmele T, Keller C, *et al*. 2003 *Astron. Nachr.* **324** 303
[9] Bettonvil F C M, Collados M, Feller A, *et al.* 2010 *Proc. SPIE* 77356, *Ground based and Airborne Instrumentation for Astronomy III*, July 20, 2010, San Diego, California, USA, p. 77356I

[10] Hofmann A and Rendtel J 2003 *Proc. SPIE* 4843*, Polarimetry in Astronomy*, February 14, 2003, Waikoloa, Hawaii, USA, p. 112
[11] Yuan S 2014 *Solar Polarization* 7, September 9–13, 2013, Kunming, China, p. 297
[12] Liu Z H, Deng Y Y, Ji H S and Li H 2012 *Sci Sin-Phys. Mech. Astron.* **42** 1282
[13] Goode P R, Coulter R, Gorceix N, *et al*. 2010 *Astron. Nachr.* **331** 620
[14] Bueno J M and Artal P 1999 *Opt. Lett.* **24** 64
[15] Bueno J M 2000 *Vision Research* **40** 3791
[16] Heredero R L, Uribe-Patarroyo N, Belenguer T, Ramos G, Sánchez A, Reina M, Pillet V M and Sálvarez-Herrero A 2007 *Appl. Opt.* **45** 689
[17] Alvarez-Herrero A, Uribe-Patarroyo N, García Parejo P, Vargas J, Heredero R L, Restrepo R, Martínez-Pillet V, del Toro Iniesta J C, López A, Fineschi S, Capobianco G, Georges M, López M, Boer G and Manolis I 2011 *Proc. SPIE* 8160*, Polarization Science and Remote Sensing V*, September 9, 2011, San Diego, California, USA, p. 81600Y
[18] 18. Stephen A D, Kyle B M and Jay E S 2004 *Proc. SPIE* 5554*, Photonics for Space Environments IX*, October 12, 2004, Bellingham, WA, USA, p. 46
[19] Robert C W, Lewis M C, Edward W T and Roger A G 1995 *Proc. SPIE* 2482*, Photonics for Space Environments III*, May 30, 1995, Orlando, FL, USA, p. 1
[20] Francis B, Marc C D, Krzysztof Z, Tomasz N, Hugo T and Irina P V 1996 *Proc. SPIE* 2811*, Photonics for Space Environments IV*, October 18, 1996, Denver, CO, USA, p. 1
[21] Steven A L, Jacob A B, Megan E T, Craig U, Elizabeth E G, Steven R C, Michael R B and William M 2009 *Opt. Eng.* **48** 114002
[22] Woehrle C D, Doyle D T, Lane S A and Christodoulou C G 2016 *IEEE Antennas and Wireless Propagation Letters* **15** 1923
[23] Oton E, Perez-Fernandez J, Lopez-Molina D, Quintana X, Oton J M and Geday M A 2015 *IEEE Photon. J.* **7** 6900909